Analytical modeling of axial coercive field in soft ferromagnetic nanocylinders

Clime, Liviu; Yelon, A.; Wu, Y.; Veres, Teodor

Publisher's version / Version de l'éditeur:
https://doi.org/10.1166/jctn.2008.014
Journal of Computational and Theoretical Nanoscience, 5, January 1, pp. 109-116, 2008

Analytical modeling of the axial coercive field in soft ferromagnetic nanocylinders

L. Clime,[1,*] A. Yelon,[2] Y. Wu,[3] and T. Veres[1]

[1]*NRC, Industrial Material Institute,*
75 Boul. de la Mortagne, Boucherville, Canada J4B 6Y4
[2]*École Polytechnique de Montréal, Département de génie physique and Regroupement québécois sur les matériaux de pointe (RQMP) CP 6097, succ. Centre-ville, Montréal, Québec, CANADA H3C 3A7*
[3]*National University of Singapore, Department of Electrical and Computer Engineering, 4 Engineering Drive 3, Singapore 117576*

(Dated: March 7, 2007)

Abstract

Axial magnetization processes in soft ferromagnetic nanodots are investigated in this paper. Under the simplifying assumption of axisymmetric vortex-like magnetic structures we find the equilibrium magnetic configuration by unidimensional numerical minimization of the magnetic Gibbs free energy. We propose a simple analytical model for the axial magnetization processes in amorphous ferromagnetic nanodots. Axial coercive field values from this analytical model are compared with those from full numerical micromagnetic simulations and good agreement is obtained. An experimental method for evaluating the exchange interactions in soft magnetic materials by using the axial magnetic loops of nanodots with different aspect ratios is proposed.

Keywords: analytical micromagnetics, ferromagnetic nanodots, magnetic vortex, coercive field, exchange constant

*Author to whom correspondence should be addressed. Present address: NRC, Industrial Material Institute, 75 Boul. de Mortagne, Boucherville, Canada J4B 6Y4. Electronic address: Liviu.Clime@imi.cnrc-nrc.gc.ca

I. INTRODUCTION

Magnetic force microscopy,[1–3] Hall magnetometry,[2] and spin-polarized scanning tunneling microscopy[4] have shown that ferromagnetic cylindrical nanoparticles often present a flux-closing vortex configuration with zero axial magnetization in the circumferential region (vortex shell) and a small region of non-zero axial magnetization at the vortex center (vortex core).[3] Accurate experimental phase diagrams of circular permalloy[5] and supermalloy[6] nanomagnets have established the range of aspect ratios in which the vortex structure becomes the most suitable magnetization state. The theoretical study of magnetization reversal in submicron cylindrical nanodots has drawn much attention because of the potential of the dot arrays as particulate recording media[7] or magnetic random access memory (MRAM).[8] Despite their accuracy, full numerical micromagnetic techniques are not suitable for modeling large scale magnetic nanostructures due to the need for large amounts of computer time and of hardware resources. In order to avoid this difficulty, simple analytical functions for the vortex magnetization state have been proposed,[9,10] and analytical models for the magnetization processes have been developed for individual nanodots[11–14] and for arrays.[12,15] Most of these studies deal with the in-plane magnetization processes, for which the reversal mechanisms consist of nucleation, displacement and annihilation of a given vortex configuration[8,11–13] whereas the out-of-plane magnetization processes have not been as thoroughly studied.

In this paper we use Usov's analytical functions[10] in order to model the out-of-plane (axial) magnetization processes in ferromagnetic nanodots with a vortex-like magnetization state. Due to axial symmetry, the vortex core displacements are completely neglected, so that the core reversal consists only of nucleation and annihilation of axisymmetric vortex states. Magnetization processes in the nanodot shell are assumed to be coherent rotations, and the vortex core radius to be invariant. Under these assumptions, the equilibrium vortex state in an external magnetic field is obtained by unidimensional minimization of the Gibbs free energy with respect to the vortex core radius. Axial magnetization processes in the nanodot shell are treated as perpendicular magnetization processes, using the Stoner-Wohlfarth model.[16] The reversal mechanism is then analytically investigated and the coercive field values corresponding to the global magnetization reversal are compared with those obtained by full numerical micromagnetic simulations.

II. NUMERICAL MICROMAGNETICS

Numerical micromagnetic simulations of axial magnetization processes in permalloy cylindrical nanodots with different aspect ratios were performed using the public code OOMMF.[17] The material parameters were those given as default for permalloy in OOMMF, that is $A = 13 \times 10^{-12} J/m$ for the exchange constant and $M_s = 0.86 \times 10^6 A/m$ for the saturation magnetization. All the nanodots have the same thickness $L = 20\,nm$ but different radii, R, from $30\,nm$ to $200\,nm$. Uniformly decreasing magnetic fields from $+2\,T$ down to $-2\,T$ by 50 equidistant steps were applied in the axial direction and the magnetic equilibrium configuration found at each field stage. Each field stage is numbered from 0 to 49 in such a way that 0 corresponds to $+2\,T$ and 49 to $-2\,T$ field values.

All the nanodots investigated exhibit a core-shell vortex structure with large values for the axial component m_z near the cylinder symmetry axis (vortex core) but considerably smaller values (even zero) in the circumferential region (vortex shell). An example of such a structure is shown in Fig. 1 for $R = 50\,nm$. The red arrows represent a vector cut plane (yOz) through the remanent magnetization field (zero applied field). The colors of the points in this plane are associated with the axial component m_z of the magnetization: blue indicates very small values ($m_z = 0$) of this parameter whereas red highlights the axially magnetized regions ($m_z \approx 1$). The color gradient corresponds to a transition region, in which the magnetization components vary continuously between the extreme values.

In order to provide a more quantitative insight into this core-shell magnetic configuration, we show, in the upper graph of Fig. 1, the dependence of both axial m_z and circumferential m_φ components along a radial direction (Oy) of the nanodot. The axial component vanishes at almost all points in the vortex shell ($|y| > R_v$) but has large values in the vortex core ($|y| < R_v$). In contrast, the circumferential component m_φ is maximal in the vortex shell but becomes continuously smaller in the vortex core, so that it completely vanishes at points located on the symmetry axis (O).

Under application of an external axial magnetic field, the topology of the magnetization profiles along the nanodot radial direction changes and the magnetization components in both core and vortex shell undergo inherent modifications. In Fig. 2 we show the profile of axial magnetization (M_z) along a radial direction of the nanodot (Oy as shown in Fig. 1) for $R = 100\,nm$. As we may see in this figure, at the first field stage (point A and $H_0 = +2\,T$)

the nanodot is completely saturated in the axial direction that is M_z equals the saturation magnetization $M_s = 0.86 \times 10^6\, A/m$ of the sample. The following field values until the 16th stage ($H_{16} = 0.72\, T$) hardly change the magnetic configuration of the nanodot but at the 17th stage (point B and $H_{17} = 0.8\, T$) a non-uniform configuration nucleates and replaces the previous uniform magnetization state.

As the magnetic field continues to decrease, the vortex core shrinks slightly and the axial magnetization in the vortex shell diminishes. Point O corresponds to the 25th field stage, with $H_{25} = 0$ that is the remanent magnetization state of the nanodot. As already shown elsewhere,[18] the axial magnetization corresponding to this remanent state is almost zero in all vortex shell points except a very small region near the vortex core where M_z is negative but much smaller than in the core so that the nanodot still has a net magnetization in the axial direction. At small negative field, the nanodot undergoes a small, continuous decrease of the core radius and an increase of the shell axial magnetization in the negative direction (process OC on Fig. 2). Because the vortex core is still magnetized in the positive direction, the total magnetic moment of the nanodot vanishes when absolute values of the vortex core and shell magnetic moments balance. Between C and D ($H_{29} = -0.32\, T$ and $H_{30} = -0.4\, T$), the vortex core undergoes a magnetization reversal. Below $-0.4\, T$, absolute values of axial magnetization increase uniformly with the same susceptibility as before, until point E. Further increases of the negative field result in annihilation of the vortex core-shell configuration, and the nanodot reaches the uniform magnetization state (point F) in the negative direction.

Four critical points may be identified in the axial magnetization process described above:

- vortex nucleation, corresponding to the transition AB from the uniform to the core-shell magnetization state;
- coercive field, where the total magnetic moment vanishes (between O and C);
- core reversal (transition CD) and
- vortex annihilation, from vortex core-shell to uniform magnetization states (EF).

Theoretical investigation of these processes may relate intrinsic properties of the ferromagnetic materials with critical fields on the magnetization loops. In Fig. 3 we show a typical magnetization curve as obtained by numerical modeling ($R = 50\, nm$). As we may

see in this figure, the most easily distinguishable critical points are the vortex nucleation (AB) and the coercive field (H_c). The vortex annihilation (EF) is satisfactorily distinguishable for this process, but it becomes very difficult to observe for large nanodots. The vortex core reversal (CD) is almost impossible to identify on the magnetization curve for all the nanodots investigated here, which cannot be used for this purpose.

In what follows, we describe an analytical model for the axial magnetization processes in soft ferromagnetic nanodots, and apply this model in order to find an expression for the axial coercive field.

III. ANALYTICAL MICROMAGNETICS

The main objective of this section is to obtain an analytical expression for the total Gibbs free energy and find the equilibrium configuration of the nanodot magnetization by numerical minimization of this energy. In order to express the terms of the Gibbs free energy we have to define analytical functions $\vec{m}(x, y, z)$ for the magnetization vector field inside the ferromagnetic nanodot. Such analytical functions for the magnetization vector inside the vortex core has been proposed by Feldtkeller and Thomas[9] and by Usov.[10] In this work we use the latter, which has been intensively applied in the last decade for in-plane magnetization processes in soft ferromagnetic nanodots.[11–13,15,18] Our choice is motivated by the fact that the magnetization states in Usov's model are described by piecewise functions whose sub-intervals correspond to the vortex core and vortex shell. Thus, we have a clear separation between the vortex core and shell so that no additional parameters are needed in order to approximate the core radius.

Usov's analytical rigid vortex model[10,11] involves two complex variables, a and c, related to the vortex core displacement x_v, and the vortex core radius R_v. For axisymmetric magnetization states a and consequently x_v are both zero, so that $R_v = cR$ with c referred to as a normalized vortex core radius. The components of the normalized magnetization at each point of a cylindrical nanodot are then given by two simplified complex functions:

$$m_{xy}(s) = \frac{2w(s)}{1 + w(s) \cdot \overline{w}(s)} \tag{1}$$

for the in-plane component, and

$$m_z(s) = \frac{1 - w(s) \cdot \overline{w}(s)}{1 + w(s) \cdot \overline{w}(s)} \tag{2}$$

for the out-of-plane (axial) component. In Eqs. (1) and (2), s is a complex number used to represent the position vector $\vec{r} = (x, y)$, defined as

$$s = \frac{x}{R} + i\frac{y}{R} \tag{3}$$

where R is the cylinder radius and $w(s)$ is a piecewise complex function:

$$w(s) = \begin{cases} i\frac{s}{c} & \text{if } |s| < c \\ i & \text{if } |s| \geqslant c. \end{cases} \tag{4}$$

We denote by $\overline{w}$ the complex conjugate of w and $i = \sqrt{-1}$.

An intuitive graphical representation of an axisymmetric vortex magnetization state obtained with the above equations is shown in Fig. 4. This configuration corresponds to a remanent state of the nanodot, that is, in zero applied field. The axial component m_z of the magnetization in this remanent state is zero at all points of the nanodot shell ($r > R_v$), but becomes large close to the cylinder axis ($r \ll R_v$). The magnetic moment in the axial direction is directly related to the core vortex radius and in the remanent state it does not depend on the vortex shell volume (in the shell, the axial component of the magnetization is zero).

In non-zero axial magnetic field, the shell magnetization changes and we assume that the magnetization is proportional to the applied field, so that

$$M_z = H. \tag{5}$$

The assumptions made in order to write Eq. (5) are that magnetization processes consist mainly of coherent rotations, described by transverse Stoner-Wohlfarth curves and are independent of the vortex core configuration. In order to illustrate the validity of this assumption, we show in Fig. 5 the dependence of the axial magnetization component M_z upon external applied field H, at a point located inside the vortex shell as obtained from numerical micromagnetic simulations. This curve corresponds to the demagnetization process shown in Fig. 2. The critical points B, O, C, D and E of this process are highlighted and labeled in Fig. 5. The dependence of the axial magnetization on external applied field is linear with

an almost unit slope (the exact value is 1.08). This justifies our assumption, and validates Eq. (5). Obviously, this equation cannot be used in describing non-equilibrium processes which imply transitions from or toward uniform magnetic states (AB or EF in Fig. 2).

We now combine Usov's analytical functions with Eq. (5) in order to obtain a complete description of the magnetization vector field inside a core-shell vortex configuration. If we define $h = H/M_s$, Eq. (5) may be rewritten as

$$m_{z,shell} = h. \tag{6}$$

We assume that the axial magnetization component (m_z) in the vortex core is given by

$$m_{z,core}(r) = (1-h)\frac{R_v^2 - r^2}{R_v^2 + r^2} + h, \tag{7}$$

that is, Usov's original analytical expression for the axial magnetization in the vortex core (2) is rescaled so that its minimal and maximal values are now h and 1 instead of 0 and 1 respectively, as in Eq. (2). A graphical representation of magnetization profiles along the nanodot radial direction, obtained from Eq. (7), is shown in Fig. 6. If the radial component of the magnetization is assumed to be zero at all points inside the nanodot then $m_z^2 + m_\varphi^2 = 1$ and the circumferential component m_φ can easily be expressed as

$$m_\varphi = \sqrt{1 - m_z^2}. \tag{8}$$

With the analytical functions of Eqs. (7) and (8) we shall deduce the total Gibbs free energy and obtain the equilibrium configuration for a vortex-like magnetic structure nucleated in an amorphous nanodot (any magnetocrystalline anisotropy contribution is neglected).

A. Exchange energy

The exchange energy functional for a ferromagnetic body of volume V is generally expressed as

$$E_{EX} = \int_V A\left[(\nabla m_x)^2 + (\nabla m_y)^2 + (\nabla m_z)^2\right] dV \tag{9}$$

were A is the exchange constant and m_x, m_y and m_z the Cartesian components of the normalized magnetization. Because the analytical expressions for the magnetization are

piecewise functions (Eqs. 6 and 7) the integral in Eq. (9) splits into two terms $E_{EX,core}$ corresponding to the vortex core and $E_{EX,shell}$ for the vortex shell so that

$$E_{EX} = E_{EX,core} + E_{EX,shell} \tag{10}$$

Using Eq. (7) for the z component and $m_x = m_\varphi \sin\varphi$ and $m_y = m_\varphi \cos\varphi$ we can easily deduce that[14]

$$E_{EX,core} = 2\pi LA \int_0^{R_v} \left[\left(\frac{\partial m_{z,core}}{\partial r} \right)^2 \frac{1}{1 - m_{z,core}^2} + \frac{1 - m_{z,core}^2}{r^2} \right] r\, dr \tag{11}$$

As for the second term, with $m_{z,shell} = h$ from Eq. (6) we simply have $m_{\varphi,shell} = \sqrt{1-h^2}$ and

$$E_{EX,shell} = 2\pi LA(1 - h^2) \ln \frac{R}{R_v}. \tag{12}$$

B. Demagnetizing energy

The energy due to the demagnetizing field of the nanodot is obtained from the distributions of the magnetic charges (poles) on the dot side and faces.[11] For an axisymmetric vortex state, the magnetization is tangential to the surface at all points on the cylinder side so that the demagnetizing energy is given by the distributions of magnetic charges on the cylinder end faces only. The contribution from the magnetic charges located on the nanodot faces is given by[11]

$$E_{MS} = \mu_0 M_s^2 \pi \left[G(0) - G(L) \right] \tag{13}$$

where

$$G(x) = \frac{1}{(2\pi)^2} \int_0^R \int_0^R \int_0^{2\pi} \int_0^{2\pi} \frac{r_1 r_2 \sigma(r_1)\sigma(r_2) dr_1 dr_2 d\varphi_1 d\varphi_2}{\sqrt{x^2 + r_1^2 + r_2^2 - 2r_1 r_2 \cos(\varphi_1 - \varphi_2)}}. \tag{14}$$

σ represents the surface density of the magnetic poles on the cylinder faces and for the magnetic configuration we proposed in Eqs. (6) and (7), it must be expressed as

$$\sigma(r) = \begin{cases} (1-h)\frac{R_v^2 - r^2}{R_v^2 + r^2} + h & \text{if } r \leqslant R_v \\ h & \text{if } r > R_v. \end{cases} \tag{15}$$

C. Zeeman energy

In a uniform axial magnetic field, the Zeeman energy functional can be expressed as a sum of two terms corresponding to the vortex core and shell regions:

$$E_Z = E_{Z,core} + E_{Z,shell} \tag{16}$$

If we denote by μ_{core} and μ_{shell} the total magnetic moments of the core and shell regions respectively, we find

$$E_Z = \mu_0 h M_s \mu_{core} + \mu_0 h M_s \mu_{shell} \tag{17}$$

with μ_0 the absolute magnetic permeability of the vacuum. We have

$$\mu_{core} = 2\pi L M_s \int_0^{R_v} m_{z,core} r dr \tag{18}$$

and the above integral can easily be carried out by taking into consideration the well known result

$$\int \frac{p - x^2}{p + x^2} x dx = -\frac{x^2}{2} + p \ln\left(p + x^2\right) + C \tag{19}$$

and obtain

$$\mu_{core} = 2\pi L R_v^2 M_s \left[h + (1 - h)\ln 2 - \frac{1}{2}\right]. \tag{20}$$

For the vortex shell we have

$$\mu_{shell} = \pi L M_s \left(R^2 - R_v^2\right) h. \tag{21}$$

D. Gibbs free energy

The total Gibbs free energy of an amorphous ferromagnetic nanodot in a vortex-like magnetization state can now be written as

$$E = E_{EX} + E_{MS} + E_Z \tag{22}$$

where the terms above are given by Eqs. (10), (13) and (16). The equilibrium configuration arises from the competition between these three terms and can be obtained by unidimensional numerical minimization of E with respect to the vortex core radius R_v i.e. by solving

$$\delta E\left(h; R_v\right) = 0. \tag{23}$$

Eq. (23) states that the core radius has to be computed at each magnetic field stage. The dependence of total Gibbs free energy E on vortex core radius R_v for axial magnetic fields from $h = -0.2$ up to $h = +0.2$ is shown in Fig. 7(a). As the magnetic field h becomes large, the vortex core radius value at which E is minimum increases continuously. The vortex core radius undergoes an absolute variation of $\Delta R_v \approx 3\,nm$ when the magnetic field changes from $h = -0.1$ to $h = +0.1$. However, for relatively small values of the axial magnetic field we can consider that the vortex radius does not vary too much with respect to the remanent state ($h = 0$) so that the energy minimization may be carried out over two energetic terms only, E_{EX} and E_{MS} ($h = 0 \Rightarrow E_Z = 0$):

$$\delta(E_{EX} + E_{MS}) = 0. \tag{24}$$

This assumption greatly simplifies the analytical modeling of the magnetization processes in weak axial magnetic fields because Eq. (23) has to be solved only once, for the remanent state, any other state being completely defined by the external field value by virtue of Eq. (6). As we shall see in the next section, this assumption is very appropriate in axial coercive field modeling, due to its relatively small values.

Accurate numerical solutions of Eq. (24) for amorphous permalloy nanodots with $L = 20\,nm$ of thickness and radius values in the range 30 to $200\,nm$ indicate that the vortex core radius is about $R_v = 15.44\,nm$ and does not depend upon dot radius (see Fig. 8(a)). The same behavior was obtained by full numerical micromagnetic modeling (OOMMF)[17] as we may see in Fig. 8(b). We show here a comparison between the remanent magnetic configurations at equilibrium as obtained with the analytical rigid vortex (ARVM) and numerical (OOMMF) models. We observe that the analytical model agrees well with the numerical simulations except in the boundary region between core and shell where the analytical model underestimates the axial magnetization component.

IV. AXIAL COERCIVE FIELD

The coercive field in an axial magnetization process is obtained by imposing the condition that the total magnetic moment of the nanodot vanishes. This condition is fulfilled when the magnetic moments of the vortex core and vortex shell are of the same magnitude but in opposite directions. Mathematically, this condition may be written as:

$$m_{z,shell}\pi L\left(R^2 - R_v^2\right) = 2\pi L \int_0^{R_v} m_{z,core} r dr. \tag{25}$$

By using the analytical expressions (6) and (7) for $m_{z,shell}$ and $m_{z,core}$ respectively, we obtain

$$H_c(R) = M_s \frac{\ln 2 - 0.5}{\frac{R^2 - R_v^2}{R_v^2} + \ln 2 - 1}. \tag{26}$$

As we may observe in Fig. 9(a), this result agrees very well with the axial coercive field from numerical micromagnetic simulations (OOMMF). That is, the axial magnetization processes are described acceptably by the analytical model.

This result may be very useful in the experimental determination of the exchange constant A by numerical fit of Eq. (26) to the experimental values of the coercive field of nanodots with different aspect ratios and R_v as fit parameter and then solving Eq. (24) with A as unknown. As an example, we show in Fig. 9(b) the solution of Eq. (24) for exchange constant values in the range of 5×10^{-12} to $12 \times 10^{-12}\, J/m$ and saturation magnetization $M_s = 0.86 \times 10^6\, A/m$.

V. CONCLUSION

Using Usov's analytical rigid vortex model we investigated the axial magnetization processes in soft ferromagnetic nanocylinders (nanodots). We deduced analytical expressions for exchange, demagnetizing and Zeeman energy terms for axisymmetric vortex configurations and obtained the equilibrium configurations by numerical minimization of the total Gibbs free energy. We propose an analytical model for the axial magnetization processes in soft ferromagnetic nanodots and find a simple analytical expression for the axial coercive field under the assumption that the vortex core exerts negligible influence on the magnetization processes in the vortex shell. Both the magnetization profiles and axial coercive fields from

this analytical model are found in good agreement with those from full numerical micromagnetic simulations. The influence of the exchange constant on the vortex core radius is investigated and the relationship between these two parameters presented for an amorphous ferromagnetic nanodot.

Acknowledgments

Authors thank Réseau québécois sur les matériaux de pointe (RQMP) for computational facilities. This work is supported by a joint grant from the Natural Sciences and Engineering Research Council and the National Research Council of Canada.

---

1. M. Natali, I. L. Prejbeanu, A. Lelib, L. D. Buda, K. Ounadjela, and Y. Chen, Phys. Rev. Lett. 88(15), 157203 (2002)
2. R. Pulwey, M. Rahm, J. Biberger, and D. Weiss, IEEE Trans. Magn. 37(4), 2076 (2001)
3. T. Shinjo, T. Okuno, R. Hassdorf, K. Shigeto, and T. Ono, Science 289, 5481 (2001)
4. A. Wachowiak, J. Wiebe, M. Bode, O. Pietzsch, M. Morgenstern, and R. Wiesendanger, Science 298, 577 (2002)
5. M. Schneider, H. Hoffmann, and J. Zweck, Appl. Phys. Lett. 77, 2909 (2000)
6. R. P. Cowburn, D. K. Koltsov, A. O. Adeyeye, M. E. Welland, and D. M. Tricker, Phys. Rev. Lett. 83, 1042 (1999)
7. E. F. Wassermann, M. Thielen, S. Kirsch, A. Pollmann, H. Weinforth, and A. Carl, J. Appl. Phys. 83(3), 1753 (1997)
8. K. L. Metlov and K. Y. Guslienko, J. Magn. Magn. Mater. 242-245, 1015 (2002)
9. E. Feldtkeller and H. Thomas, Phys. Kondens. Mater. 4, 8 (1965)
10. N. A. Usov and S. E. Peschany, J. Magn. Magn. Mater. 118, L290 (1993)
11. K. Y. Guslienko and K. L. Metlov, Phys. Rev. B 63, 100403(R) (2001)
12. K. Y. Guslienko, V. Novosad, Y. Otani, H. Shima, and K. Fukamichi, Phys. Rev. B 65, 024414 (2001)
13. K. Y. Guslienko, V. Novosad, Y. Otani, H. Shima, and K. Fukamichi, Appl. Phys. Lett. 78(24), 3848 (2001)

14. P.-O. Jubert and R. Allenspach, Phys. Rev. B 70, 144402 (2004)

15. Y. B. Grebenshchikov and N. A. Usov, J. Appl. Phys. 93(8), 4810 (2003)

16. E. C. Stoner and E. P. Wohlfarth, IEEE Trans. Magn. 27, 3475 (1991)

17. M. J. Donahue and D. G. Porter, Oommf user's guide, version 1.0, Technical Report NISTIR 6376, National Institute of Standards and Technology (1999)

18. W. Scholz, K. Y. Guslienko, V. Novosad, D. Suess, T. Schrefl, R. W. Chantrell, and J. Fidler, J. Magn. Magn. Mater. 266(1-2), 155 (2003)

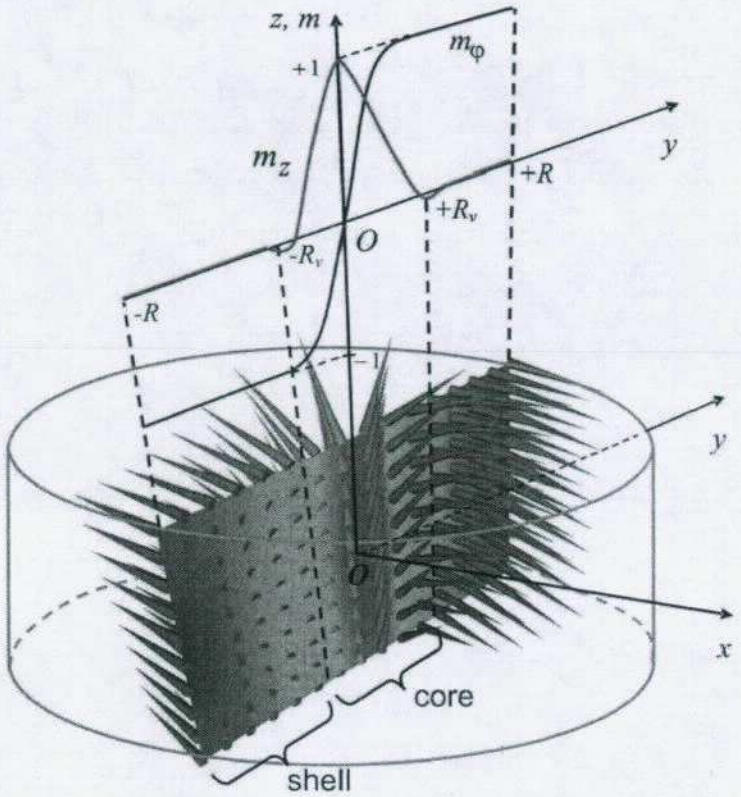

FIG. 1: Vector cut plane of the remanent magnetization state in a permalloy ferromagnetic nanodot and magnetization profiles along the nanodot radial direction Oy for the components m_z (red) and m_φ (blue) as obtained by numerical micromagnetic simulation.

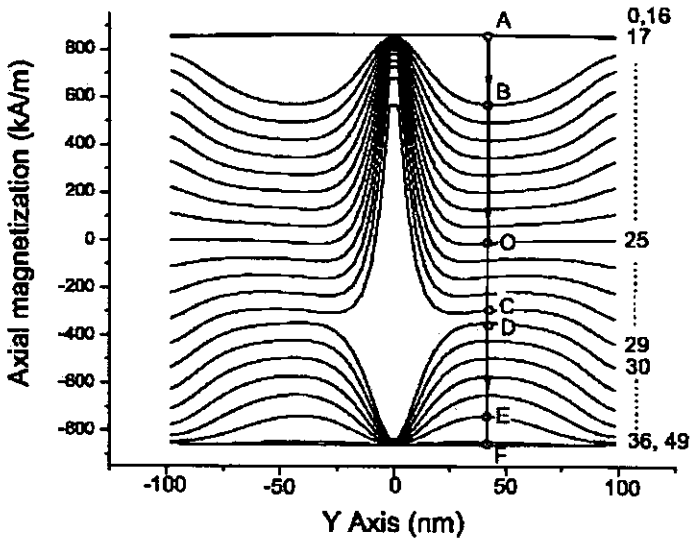

FIG. 2: Axial magnetization (M_z) along the radial direction Oy (as shown in Fig. 1) for a permalloy nanodot with $R = 100\,nm$ and magnetic fields uniformly decreased from $+2\,T$ to $-2\,T$ in 50 equal steps. Magnetic field stages are numbered with integers from 0 (corresponding to $+2\,T$) to 49 (for $-2\,T$). Some of these numbers are indicated to the right of the curves.

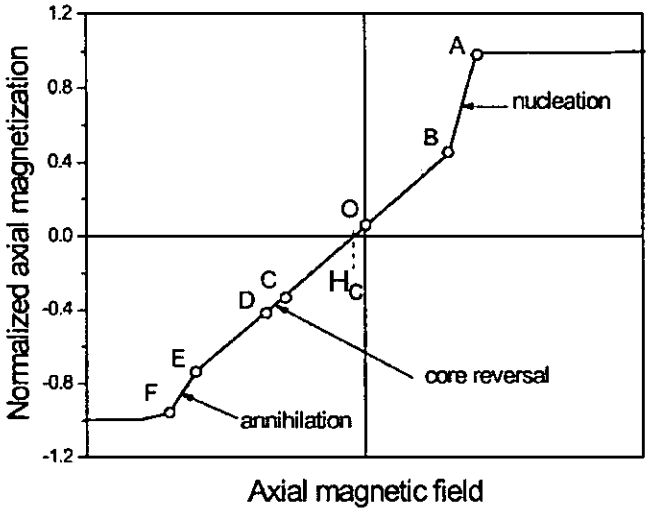

FIG. 3: Typical axial demagnetization curve for an amorphous ferromagnetic nanodot of radius $R = 50\,nm$.

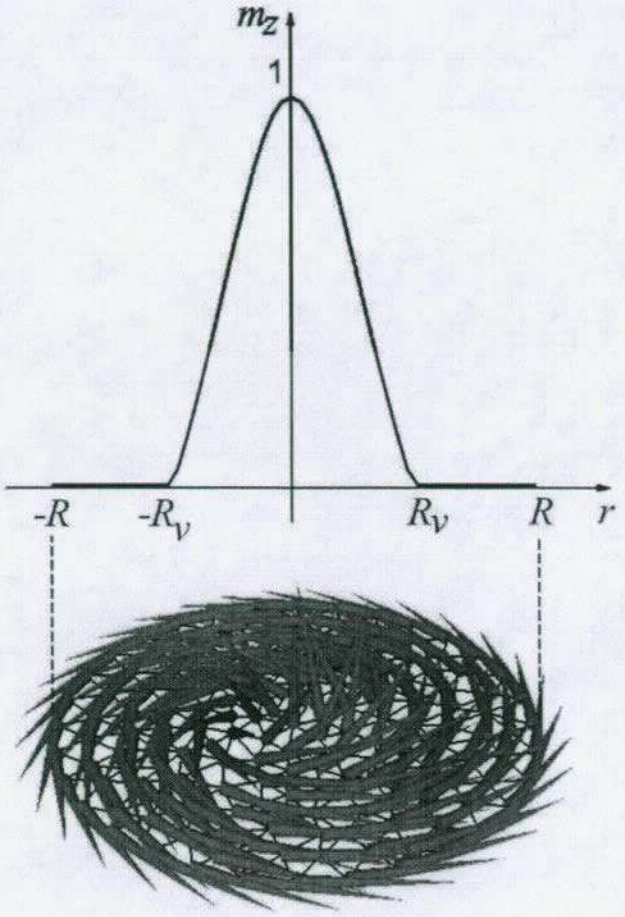

FIG. 4: Remanent magnetization state in a cylindrical ferromagnetic nanodot for an axisymmetric vortex state as obtained with the analytical rigid vortex model for $R_v = 0.5R$.

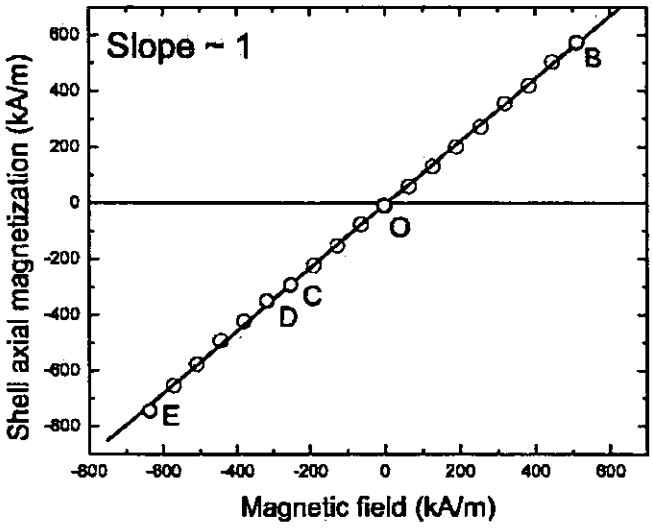

FIG. 5: Dependence of the axial magnetization (M_z) in the vortex shell on the external applied magnetic field.

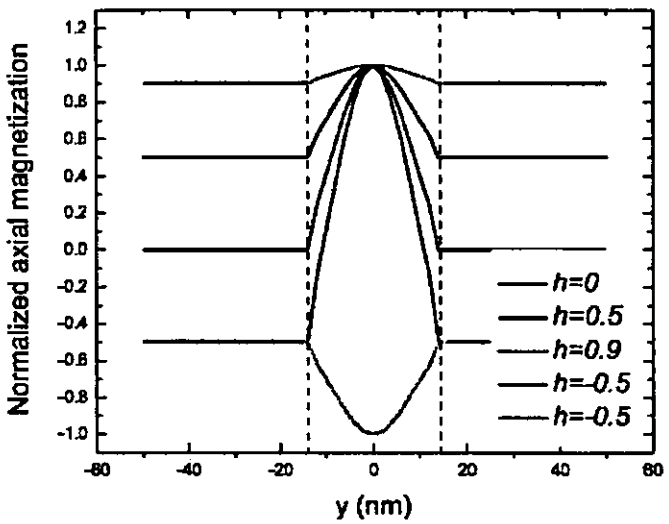

FIG. 6: Axial magnetization profile along the radial direction Oy (Fig. 1) as obtained with the analytical rigid vortex model - Eq. (7) - for four values of the external magnetic field and $R_v = 15.44\,nm$. At $h = -0.5$ both parallel (cyan) and antiparallel (blue) magnetic configurations are shown.

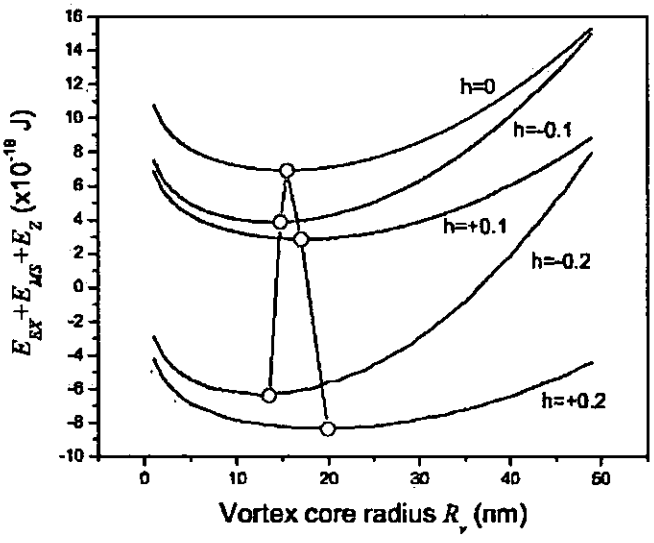

FIG. 7: Dependence of total Gibbs free energy on vortex core radius R_v for a nanodot with $R = 100\,nm$ of radius at various positive and negative applied magnetic fields. Open symbols indicate the position of the energy minimum on each curve.

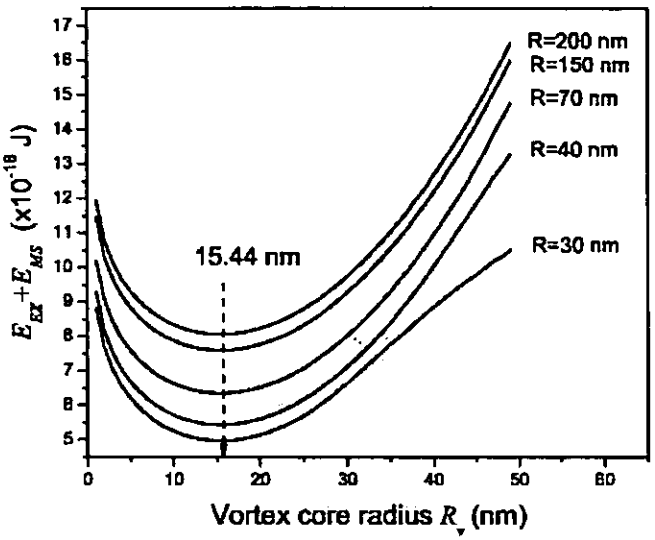

(a)

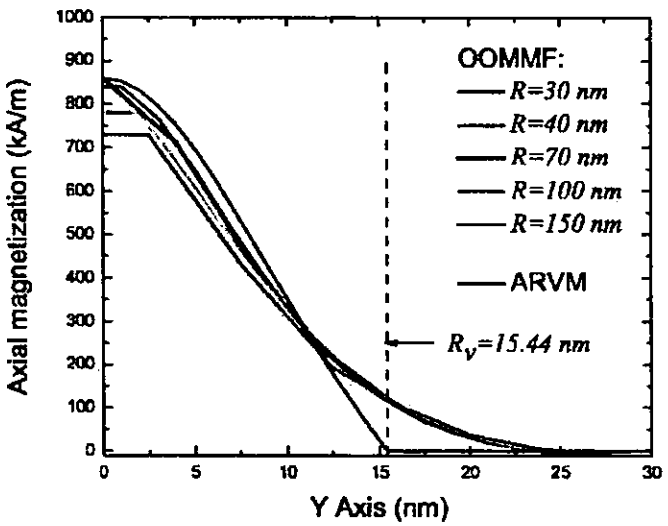

(b)

FIG. 8: (a) Analytical modeling of total Gibbs free energy dependence on vortex core radius of nanodots of thickness $L = 20\,nm$ and various radii from $R = 30\,nm$ up to $R = 200\,nm$ in the absence of an external magnetic field; (b) Numerical and analytical micromagnetic simulations of the remanent axial magnetization (m_z) in permalloy nanodots with different aspect ratios ($L = 20\,nm$).

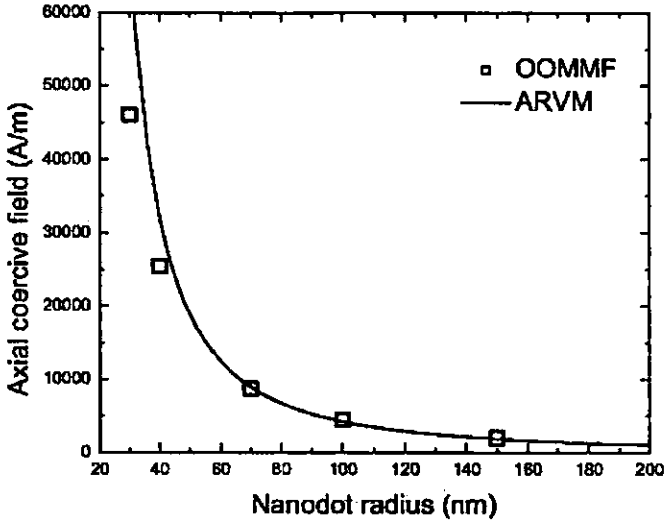

(a)

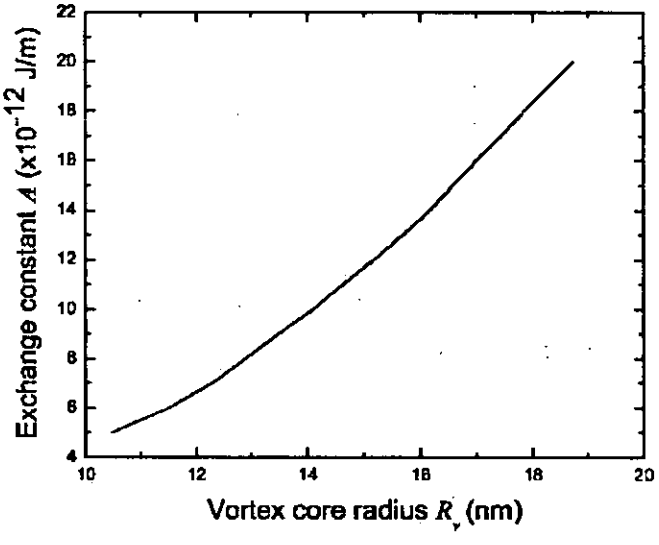

(b)

FIG. 9: (a) Numerical (symbols) and analytical (line) modeling of the axial coercive field for circular permalloy nanodots with $L = 20\,nm$ and radius from 25 up to $200\,nm$; (b) Solution of Eq.(24) for exchange constant values in the range of 5×10^{-12} to $12 \times 10^{-12}\,J/m$.